Nanoscale

Gallium-Indium Nanoparticles as Phase Change Material Additives for Tunable Thermal Fluids

Journal:	*Nanoscale*
Manuscript ID	NR-COM-09-2020-006526.R1
Article Type:	Communication
Date Submitted by the Author:	23-Nov-2020
Complete List of Authors:	Mingear, Jacob; Texas A&M University System Farrell, Zachary; UES Inc; US Air Force Research Laboratory Hartl, Darren; Texas A&M University System, Tabor, Christopher; US Air Force Research Laboratory,

Article type: Communication

Gallium-Indium Nanoparticles as Phase Change Material Additives for Tunable Thermal Fluids

Jacob Mingear, Zachary Farrell, Darren Hartl, Christopher Tabor*

Jacob Mingear, Prof. Darren Hartl

Department of Aerospace Engineering, Texas A&M University, 3141 TAMU, College Station, TX 77843, USA

Dr. Zachary Farrell

UES, Inc., Dayton, OH 45432

Materials and Manufacturing Directorate, Air Force Research Laboratory, Wright Patterson Air Force Base, OH 45433, USA

Dr. Christopher Tabor

Materials and Manufacturing Directorate, Air Force Research Laboratory, Wright Patterson Air Force Base, OH 45433, USA

christopher.tabor.1@us.af.mil

Keywords: gallium-indium alloy, liquid metal, phase change material, nanofluid, phase equilibria

Abstract

One of the most critical limitations for high-power electronics today is thermal management and routing thermal energy efficiently away from thermally sensitive components. A potential solution to this problem is the integration of cooling channels in close proximity to thermally sensitive materials for increased heat removal efficiency. These channels typically use single phase fluids (liquid), dual phase fluids (vapor-liquid), or suspended organic / polymer phase change material particles in a fluid (PCM slurry). Expanding upon the latter, this work demonstrates the use of inorganic Ga-In alloy nanoparticles (NPs) suspended in a traditional thermal transport fluid to simultaneously (1) increase the overall thermal diffusivity of the fluid and (2) serve as a cyclable solid-liquid PCM slurry which provides a thermal sink that is definable over a wide range of relevant temperatures for power electronics. Herein, the relationship between particle size, composition, and volume fraction are explored as they relate to the PCM slurry optimum working temperature, total energy absorption, and rheological properties. A mere 0.10 volume fraction of Ga-In NPs is reported to increase the overall thermal conductivity by nearly 50% and can be optimized to change phase at temperatures as low as -46°C. Based on thermal measurements, it was observed that these nanoparticle systems lack the preference to form αGa and have a large thermal hysteresis due to exhibiting extreme undercooling, with crystallization temperatures near -130°C, enabling opportunities within extreme environments such as space applications or low temperature imaging systems.

Main Text:

Miniaturization and increased power requirements in electronics, communication, and computing technologies have led to critical thermal management obstacles that call for innovative cooling technologies [1]. Integrated cooling channels in proximity to high-power thermal loads, utilizing conventional heat-transfer fluids or thermal fluids (e.g. siloxane-based oils, ethylene glycol, and water) effectively move thermal energy away from temperature sensitive electronics [2]. To increase this effect, a vaporization and condensation cycle within a fluid channel has been shown to supply a secondary thermodynamic pathway to remove heat. While vaporization of a single fluid system has been demonstrated many times and can even lead to a self-oscillating behavior [3], this approach requires significantly strengthened microchannels and additional engineering to contain the higher pressure fluxuations.

Two orthogonal approaches have been applied previously to increase the total amount of energy that can be moved away from a surface in these heat pipes by adding particulate materials to the fluids. The first approach utilizes inorganic high thermal conductivity particulate additives suspended in traditional thermal fluids, such as Ag, Au, CuO, SiO_2, or Al_2O_3. Referred to as nanofluids, this solution typically increases the average thermal conductivity of the fluid up to 20% with nanoparticle concentrations between 1-5 vol.% [4]–[6]. These nanofluids trade-off an intrinsic decrease in overall specific heat capacity relative to the pure thermal fluid resulting from the intrinsic material properties of the nanoparticles themselves. A second approach utilizes a suspended phase change material (PCM) particulate to increase the thermal capacity of the fluid. Similar to the vapor-to-liquid phase change mentioned above, a solid-to-liquid transformations can also be utilized to take advantage of an additional heat absorption mechanism – the latent heat of fusion. Often a slurry of microencapsulated PCM particles, such as paraffin or other low melting point organic materials, is suspended in a continuous fluid medium [7]–[11]. While this relaxes constraints on the engineering of the microchannels because of the lack of pressure variation, several

disadvantages exist with this approach. First, the heat of fusion tends to be roughly an order of magnitude lower than the heat of vaporization. Secondly, the PCMs are typically composed of a low molecular weight polymer or long alkane chain hydrocarbon [8] with an encapsulate shell generally composed of a thin polymer shell such as polystyrene, a formaldehyde, or a methacrylate variant [9]. These organic materials typically have a relatively low thermal conductivity. To overcome this, a few inorganic core materials such as salt hydrates [10][12] and low melting point alloys have been explored for microencapsulated PCMs [13][14].

Low melting point metals such as gallium-based and indium-based alloys have specifically seen a surge in exploration [15] for applications ranging from flexible [16] and self-healing electronics [17], reconfigurable antennas [18], heat-free solders [19], [20], electrical conformal interfaces [21], thermal interface materials [22], [23], and as a unary heat transfer fluid in shape memory applications [24] due to both their fluidic behavior and high thermal conductivities. Gallium-indium alloys are readily formulated into nanoparticles through ultrasonication with the help of a spontaneously formed native gallium oxide layer on the surface. This oxide matures to a thickness around three nanometers over the course of a month [25] [26] and passivates the colloidal nanoparticles against complete oxidation as well as preventing coalescence [25]. Once fabricated, these particles provide a colloidal suspension that lends itself to additive manufacturing processes [27], responsive self-healing circuits [28], and novel stretchable electronics [16].

In this work, we utilize colloidal nanophase gallium-indium alloys to generate an inorganic microencapsulate PCM slurry, which provides higher thermal conductivity over organic microencapsulated PCMs in addition to superior latent heat thermal properties. The thermodynamic phase diagram for colloidal nanoparticles of a size D_V50 = 90 nm is reported, and the effect of particle size and composition are explored as variables to tune the thermal behavior within a heat transfer fluid.

Gallium-indium (Ga-In) nanoparticles are fabricated utilizing previously reported techniques through ultrasonication [25], [29], [30]. A representative transmission electron micrograph image is shown in **Figure 1A**, along with a schematic of the preparation of core/shell Ga-In nanoparticles with the intrinsically formed ~3 nm gallium oxide shell [25], [31]. As previously reported, increased sonication time leads to smaller nanoparticles with a tighter log-normal size distribution [26], [29], which is corroborated by the number distributions explained via **Figure S1 to S5** across a range of 10 min to 18 h of sonication. As thermal properties are a function of volume, the particle distributions were further calculated based on their respective volume distribution [32] and are reported in **Figure 1B**. These volume distributions along with volumetric cumulative distribution medians (D_V50) shown in **Figure 1C** enable the thermal properties of the particles and the PCM slurry to be reported in a more direct approach than using number-based distributions. Further particle distribution metrologies are discussed in the supplemental information and in sources [33], [34].

To generate a suitable PCM slurry, the gallium-indium nanoparticles were suspended in AR-200 silicone oil, a typical heat exchange fluid. Parallel plate rheology was performed on a Ga-In nanoparticle (25 wt.% In) / AR-200 silicone oil slurry. **Figure 1D** shows the rheological behavior with nanoparticles loaded from 0 - 50 vol.%. Within the measured range of shear rates (1-1000 s^{-1}), the pure silicone oil (no particles) responds in a relatively Newtonian manner. As the particle loading is increased the fluid displays both an increase in low-shear viscosity and shear thinning behavior, as expected from nanoparticle loaded fluids [35]. A steep rise in the low-shear viscosity with nanoparticle loading indicates a possible gelation point after 10 vol.% NP. The PCM slurries with a loading at or below 10 vol.% began approaching the viscosity of pure silicone oil above a shear rate of 200 s^{-1}.

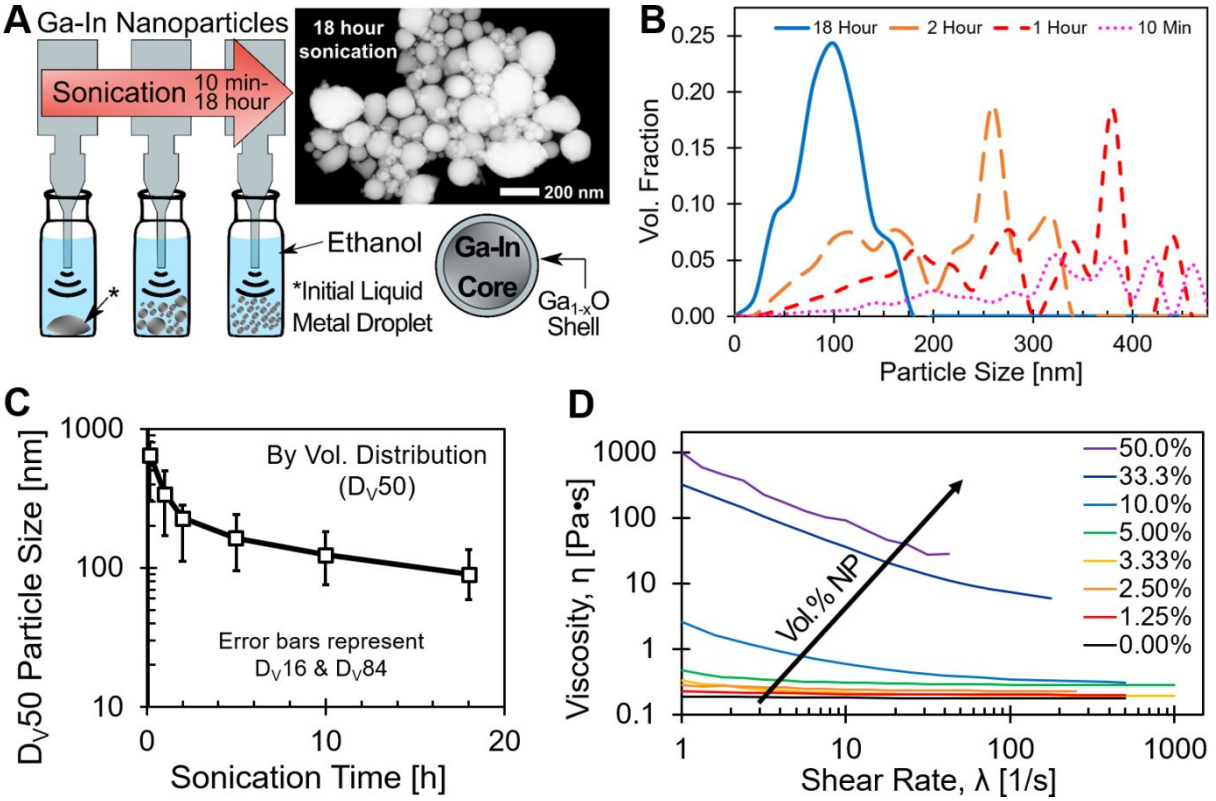

Figure 1. A Representative TEM micrograph of Ga-In nanoparticles with a schematic representation of a core/shell particle fabricated through ultrasonication process. **B** Nanoparticle size distribution by volume fraction (bin of 20); volume-weighted distributions describe thermal properties more accurately than number-weighted distribution, which is further discussed in **Figure S1** to **S5**. After 5 hours of sonication, distributions were relatively similar through 18 h samples. **C** Particle size determined via the median of the volume distribution (D_V50) in **B** over sonication time. Error bars represent D_V84 and D_V16. **D** Rheological measurements of gallium-indium nanoparticles (25 wt.% In) suspended in AR-200; with increased loadings, the fluid has an increased shear-thinning behavior.

Differential Scanning Calorimetry (DSC) was performed on several Ga-In nanoparticles in AR 200 silicone oil and bulk Ga-In alloys with varied compositions from pure Ga particles to 40 wt.% In (5°C/min ramp rates, 18 h sonication times, 5 vol.% NP in AR-200). The heating and cooling curves with various phase transitions are shown in **Figures 2A and B**, respectively; note the glass transition around -95°C from the AR-200 silicone oil. Bulk alloy measurements are provided in **Figure S6** in the supplemental information.

Pure gallium has multiple reported metastable phases, with at least six being identified from β to η at standard pressures [36], [37]. Multiple investigators have been able to reversibly form these phases when gallium or gallium alloys are confined to nanoparticles [38][39][40][41]. For

pure gallium nanoparticles, the particle sizes (which varied between 100-1000 nm) have demonstrated some correlation to certain size-dependent phases upon solidification [38][39][40]. When a wide distribution of sizes was used, this enabled multiple phases to crystallize for a single solution of particles. Upon heating those samples, the thermal data suggested that particles would melt depending on their respective crystallized phase (β, δ, λ) and resulted in multiple peaks for a given solution of particles. In contrast, Figure 2B of this work shows the pure Ga (red) nanoparticles only producing a single peak upon heating beginning around -31°C. We attribute this observation to both a smaller particle size and narrower size distribution compared to that of the previously mentioned researchers (D_V50 = 90 nm with a D_V16 = 59 nm and D_V84 and = 136 nm or an arithmetic number mean of 33 ± 27 nm). However, the melting point of -31°C for these pure Ga nanoparticles do not match the melting point of an established metastable phase (discussed later).

The thermodynamic stability of these polymorphs are also likely impacted when gallium is mixed with other elements, such as indium in this study. This is investigated in Figure 2A and 2B through further DSC analysis as larger amounts of indium are added to the initial alloy mixture prior to particle formation. Due to the narrow size distribution used here, an assumption was made that the majority of the particles undergo similar thermodynamic behavior without significant size dependent phase formation within a single solution. From this DSC data, **Figure 2C** was constructed based on the observed thermal events determined from heating DSC curves to construct a "nanophase" diagram for particles of D_V50 = 90 nm, using previously reported methods [42]. Only heating curves are needed for this construction and thermal event values are based on the onset of the solidus and the peak of the liquidus; these points are indicated by an arrow in Figure 2B. For binary eutectic phase diagrams, eutectic compositions will have a single melting point; thus, a single peak will be observed via DSC. In contrast, off-eutectic alloys will undergo imminent melting of one of the two phases of the alloy followed by the

continuous melting of the remaining phase as long as temperature is continuously increasing. Due to the significant hysteretic behavior of these particles, it would be of interest to also show where the cooling thermal events aligned on this nanophase diagram, which has additionally been added to Figure 2C. The experimentally produced diagram also contains an underlay of the bulk (αGa)-In system (solid black lines) compiled by Anderson & Ansara [43]. Note that the so-called metastable γGa-In phase diagram from [43] is not included in our discussion, as we believe that it may be erroneously based on source [44] which is on the topic of high-pressure gallium phases. Further, we stop short of identifying specific phases in these systems and reserve that for future work beyond the scope of this study. However, the general shifts in phase behavior in nanoparticle PCM slurries have several contributing mechanisms which we will go over briefly below.

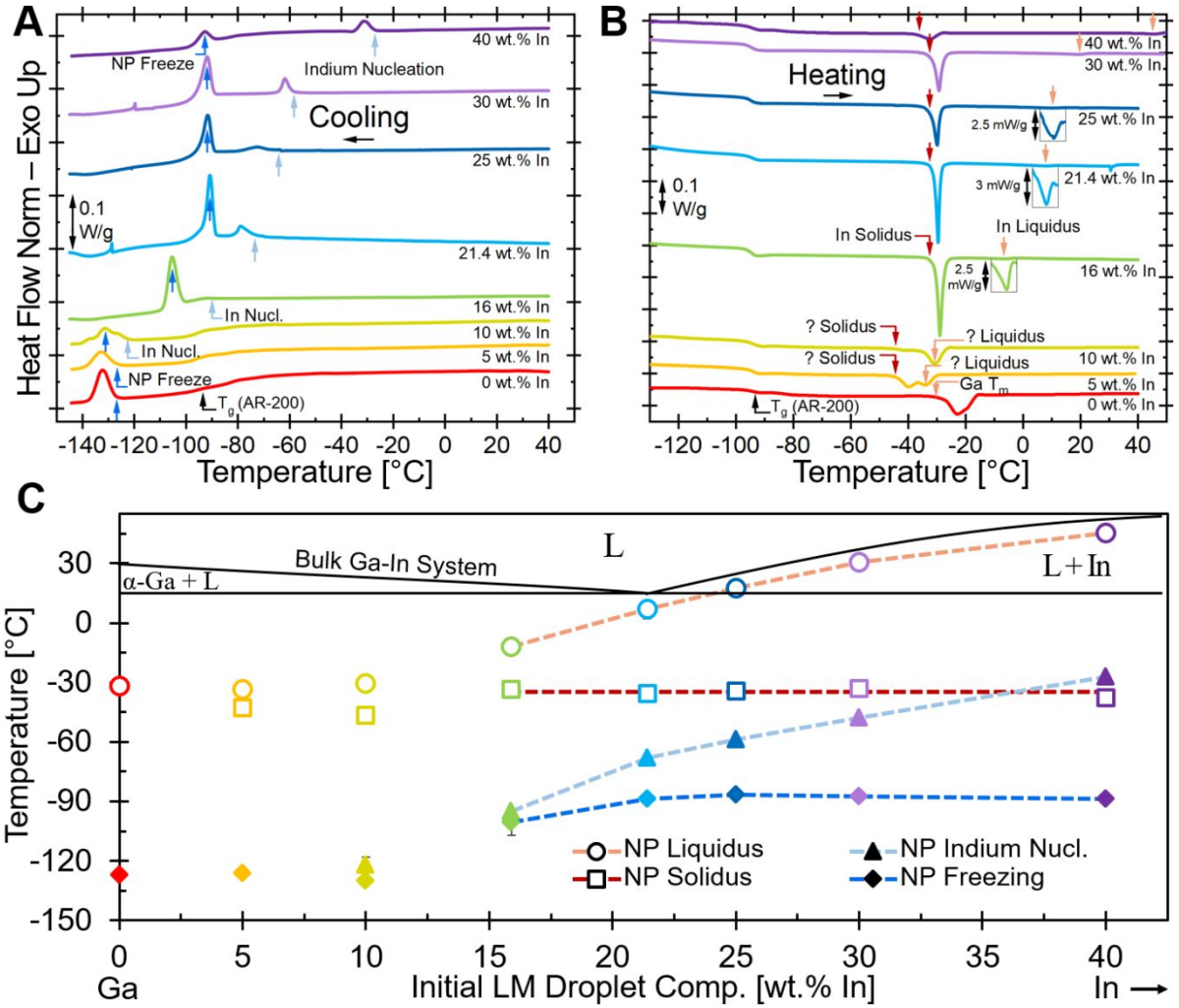

Figure 2. DSC heating (**A**) and cooling (**B**) curves of various Ga-In nanoparticle compositions used to construct a nanoparticle phase diagram (**C**) with the bulk (αGa)-In phase diagram underlaid in black lines. Phase equilibria is unclear between 0 and 16 wt.% In, but multiple phenomena are responsible for the disparate diagrams between the bulk and nanoparticle system, discussed in text. Peaks from cooling curves were added to C to highlight the extreme undercooling behavior of Ga-In nanoparticles.

This nanophase diagram is useful for understanding the phase transformations of these PCM slurries based on liquid metal composition. The thermodynamic phase equilibria of nanoalloys have been explored before in other systems [45], which usually differ substantially from their bulk counterparts. The presented diagram reflects this shift in thermodynamic properties, as the nanophase behavior clearly does not correspond to the bulk (αGa)-In system. It is clear from the nanophase diagram produced in Figure 2C, the bulk phase eutectic point at 21.4 wt.% In does not exist as a eutectic point in the nanophase, as two distinct peaks are observed in both the DSC cooling and heating curves. We have identified four phenomena that

are responsible for the significant shifts in the thermodynamic behavior of the Ga-In alloy nanoparticles: extreme undercooling, metastable phase formation, metal leaching due to oxide, and melting point depression due to high surface-to-volume ratios.

Extreme undercooling of the Ga-In nanoparticles is overtly present in the DSC cooling spectra of Figure 2A. Undercooling occurs readily in both bulk (see Fig. S6) and nanoscale gallium; however, this effect is much more prominent with the latter as defects leading to nucleation and freezing only result in the freezing of the individual particle that held the defect and not the entire volume of the various Ga-In particles. The amorphous gallium-oxide shell, further helps to insulate the particle from other external nucleating stimuli. This extreme undercooling for single component nanoparticles has been reported before by several groups [39][46][47][48], sometimes reaching as low as -180°C for 3 to 15 nm pure Ga particles [38]. Upon cooling, our In ≥ 16 wt.% cooling curves have two peaks, corresponding to nucleation of indium prior to full alloy freezing around -90°C to -100°C, as is compatible with previous work identifying the initial nucleation of indium crystals by in-situ transmission electron microscopy [41]. As the indium content is increased, the separation between the two peaks is further exaggerated as indium begins to nucleate at higher temperatures; the final freezing temperature of the entire particles remaining relatively constant between -90°C to -100°C. Interestingly, particles with an indium content below 16 wt.% In exhibit a single peak at a much lower temperature of around -130°C. It is possible that the presence of indium crystals first solidifying within the ≥16 wt.% In nanoparticles may serve as a nucleation site that enables the full crystallization of a particle at the higher temperatures. Regardless, due to these extremely low temperatures in which these nanoparticles freeze, it is believed that this allows the highly kinetic liquid to be undercooled into a regime where a nonstandard phase may be more thermodynamically stable, the implications of which are now discussed next.

The second phenomenon driving the novel nanophase thermodynamic behavior is the

potential for nanoparticles to crystallize into previously inaccessible phase morphologies [49]. As discussed earlier, multiple established metastable phases of pure Ga exist, listed here in order of decreasing melting point: βGa (T_m = -16°C), δGa (T_m = -19°C), εGa (T_m = -28°C), γGa (T_m = -35°C) [37]. The declared melting point of pure Ga nanoparticles in this work (~ -31°C) does not precisely match thetemperature of these previous works. It may be the εGa phase and the resulting 3°C difference is due to melting point depression as discussed in a following section. While the enthalpy of fusion of αGa is ~80 J/g, enthalpies of fusion for the established metastable phases are too similar (between 35-38 J/g) [37] to help elucidate phase state. With each incremental addition of In, the heating curves in Figure 2B appear to show typical solidus and liquidus peaks. Within a binary alloy such as the (αGa)-In system underlaid in Figure 2C, the eutectic isotherm (horizontal solidus line) is colinear between either side of the eutectic invariant point [50]. The solidus peaks between the cluster of 5 wt.% In, 10 wt.% In, and the cluster of 16 to 40 wt.% In declared herein are not colinear; there is a ~15°C offset in the isotherms in these two regions. Upon cooling, a 40°C discrepancy exists between the full crystallization temperatures of the above compositions which further reinforces a difference in thermodynamic behavior between high In content (≥16 wt.%) and low In content (≤10wt.%). Due to the different temperatures in which these particles fully solidify, it is suggested here that these particles are forming different gallium-rich phases during cooling, which ultimately produce disparate solidus lines similar to those observed in a work investigating high-pressure Ga metastable phases with additions of In [44]. Thus, we believe the temperature at which the particles fully solidify governs the phase structure and ultimately corresponds to observed melting/solidus/liquidus peaks upon heat-up. However, these conclusions would need to be verified through in-situ TEM diffraction and/or XRD, which is outside the scope of the current study.

The third proposed phenomenon originates from the thin (3 nm) passivating oxide shell

leaching gallium from the liquid metal core. It has been shown elsewhere that this oxide is solely composed of gallium-based oxides due to the more negative oxidation potential of gallium compared to indium [25]. This results in the oxide preferentially striping gallium from the alloy core thereby increasing its indium content in the metallic core as particle size decreases. This can become a significant effect as the particles become smaller in dimension, as has been shown previously [26]. **Figure 3A** shows the resulting computed compositional shift in the alloy nanoparticle core as a function of NP size due to the leaching of gallium from the core to generate the gallium oxide shell, which is estimated at 3 nm thickness. For example, a 300 nm diameter nanoparticle with an initial core composition of 75 wt.% Ga / 25 wt.% In will have enough gallium removed from the core to generate a 3 nm oxide shell to increase the In content of the core by only ~0.5 wt.% compared to the initial composition. This compositional shift of the alloy augments as the particles become smaller; a 50 nm diameter nanoparticle with the same initial composition has an increase in the In content of the core by ~3.25 wt.%. For the presented work, this effect could lead to a small deviation from expected thermodynamic properties (D_V50 of 90 nm results in an increase of core In composition by < 2 wt.% for most compositions).

The fourth proposed phenomenon is the depression of the melting point for a given particle size as a result of high surface-to-volume ratios at the nanoscale. Using three published thermodynamic models of nanophase melting point depression, (i.e.,Homogenous Melting Model, Liquid Shell Model, and the Liquid Nucleation and Growth Model [51]–[53]) the predicted melting point depression as a function of particle size for pure Ga is calculated in **Figure 3B** (the equations can be found in **Equation S7** and **S8)**. For the volume-weighted D_V50 particle sizes of 90 nm used in this work, these models suggest that the melting point depression due to nanoscale confinement effects can contribute up to a 15°C reduction in melting point. This effect may be manifested to a reduced degree as the 3°C drop between the pure Ga

nanoparticles melting point of -31°C and the expected melting point of the εGa of -28°C (or it may have an even greater impact as a 12°C drop between the δGa of -19°C). Similar to the oxide leaching effect mentioned above, this contribution would be more exaggerated for smaller particle sizes (especially 25 nm or less).

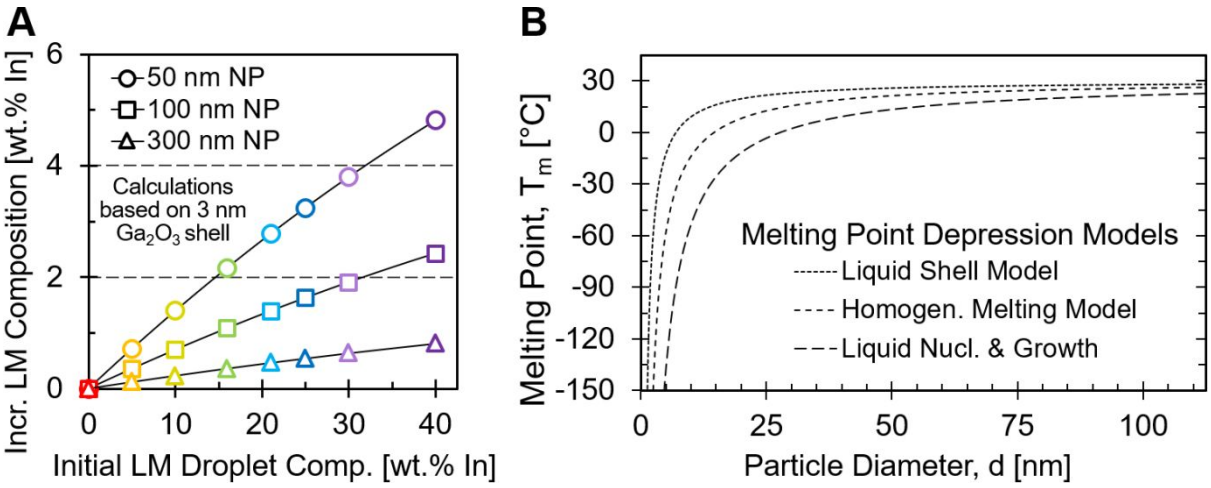

Figure 3: (**A**) Calculations for the composition change of Ga-In NP core from the creation of a gallium oxide shell. **(B)** Predicted effect of particle size on melting point depression based on three published models: the Liquid Shell Model, the Homogenous Melting Model, and the Liquid Nucleation and Growth Model.

To demonstrate the improvement in thermal properties of Ga-In PCM thermal fluids, the thermal conductivity, heat capacity, thermal diffusivity, and increase in cumulative enthalpy due to phase change were measured as nanoparticle concentration was increased in AR-200 for two use-cases: an isothermal condition (where the temperature was kept at 24°C, and thus no phase change); and a cyclic condition (where the change in temperature resulted in Ga-In NPs melting).

Thermal conductivity measurements of an isothermal condition at 24°C are shown in **Figure 4A**, which highlights a near 50% increase for a 10 vol.% loading of liquid-phase Ga-In particles in AR-200. The experimentally obtained thermal conductivity data correlates with the calculated Maxwell-Eucken relationship from effective medium theory for dilute particle dispersions [8], [54], detailed in supplemental information **Equation S2**. This increase would

be independent of the nanoparticle phase state as both solid and liquid phases have nearly equivalent thermal conductivities (~30 and 34 W/m K, respectively) [55].

Isothermal heat capacities were measured using modulated heat flow DSC at room-temperature. The components of the slurry (AR-200 and bulk Ga-In at 25 wt.% In) were measured to have volumetric specific heat capacities of 2.05 $Jcm^{-3}K^{-1}$ (1.95 $Jg^{-1}K^{-1}$) and 2.15 $Jcm^{-3}K^{-1}$ (0.34 $Jg^{-1}K^{-1}$), respectively. The addition of Ga-In nanoparticles to AR-200 results in a nearly equivalent volumetric system heat capacity for an isothermal condition, as expected. These values are shown in **Figure 4B** along with the calculated predictions based on a linear rule of mixtures, which show good agreement.

A common metric used to evaluate the utility of a thermal fluid is thermal diffusivity, presented by Equation 1:

$$\alpha = \frac{\lambda}{\rho c} (1);$$

where α is thermal diffusivity, λ is thermal conductivity, c is the heat capacity (mass), and ρ is density. The thermal diffusivities for various particle concentrations were extrapolated based on the previous measurements and are plotted in **Figure 4C**. The increase in thermal conductivity and maintained volumetric heat capacity expectedly results in higher thermal diffusivities. The increase in isothermal diffusivity in this work is beneficial and unique within PCM slurries, as most other slurries utilize a low thermally conductive organic-based phase change material that results in a decreased aggregate isothermal diffusivity. For a cyclic condition, melting would further increase in the cumulative amount of thermal energy absorbed. To show this benefit, **Figure 4D** was produced with -40°C as the initial condition; upon reaching the solidus point for NPs (25 wt.% In), an addition of thermal energy is absorbed compared to pure AR-200. Increasing the vol.% of nanoparticles accentuates this effect. Since the isothermal volumetric heat capacity with the addition of nanoparticle concentration is effectively maintained (Figure 4B), the only consequence present is the higher viscosity as

discussed in Figure 1D. In practice, the initial composition can be tuned to align the significant increase in thermal energy absorption to coincide with desired threshold temperatures.

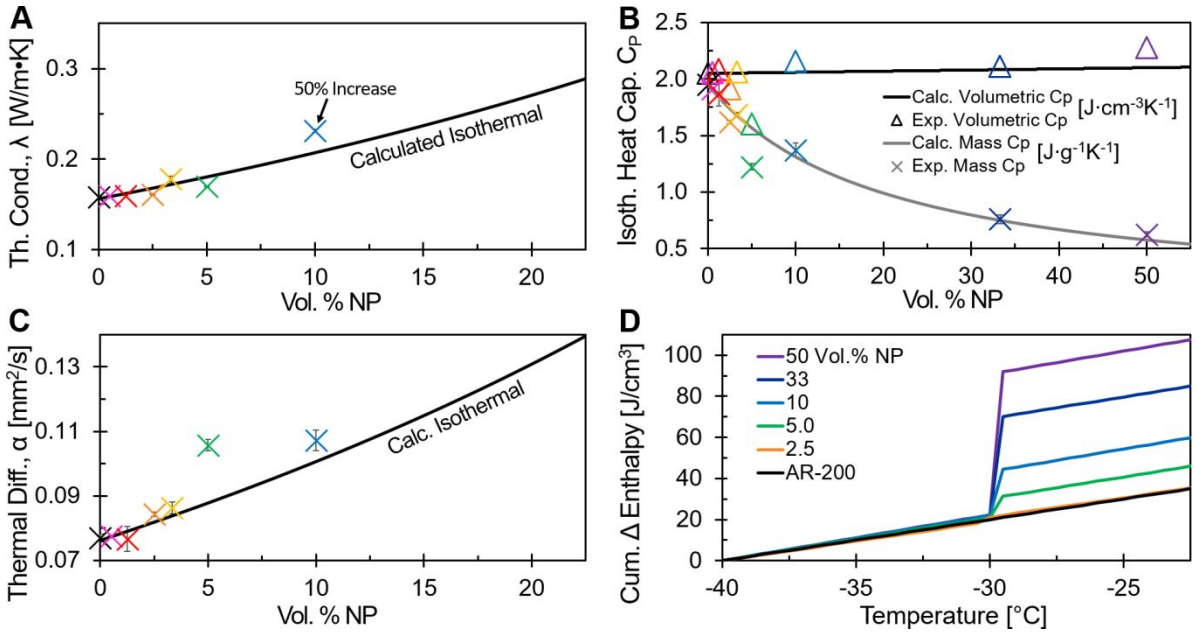

Figure 4. For Ga-In (18 h sonication, 25 wt.% In) alloy in AR-200, **A** thermal conductivity, **B** isothermal heat capacity, **C** and thermal diffusivity trends over a range of NP volume fractions. **D** The cumulative stored thermal energy starting at -40°C from including the increased energy from phase change.

In conclusion, gallium-indium nanoparticles were suspended in a typical thermal fluid(AR-200 silicone oil) to demonstrate improved thermal diffusivity and energy storage as a tunable temperature PCM slurry. The thermodynamic properties of these tunable Ga-In nanoparticles were explored and enabled the construction of a nanophase diagram for a narrow size distribution of particles with a D_V50 of 90 nm. Four independent phenomena resulted in deviations from the bulk Ga-In phase diagram, summarized below:

1. Extreme undercooling suppresses the freezing point of the particles to at most -130°C, or nearly 150°C below bulk melting. This is likely due to the low volume per particle and isolated protective conditions enabled by particle surface oxides. Further, this effect causes particles to freeze into nonstandard phases.
2. The common αGa phase no longer forms for the produced particles system; instead, uncharacterized metastable phases are produced based on composition as shown by

significant disparatity in melting/solidus/liquidus points.

3. The formation of a surface oxide preferentially removes gallium from the gallium-indium core, shifting the core composition toward indium-rich compositions; this would be exaggerated in smaller particles below 50 nm in diameter.
4. High surface-to-volume ratios at the nanoscale intrinsically depress the melting point of the particles; this contribution would be more significant at particle diameters below 25 nm.

Additional phase diagrams could be constructed with Ga-In particles at different sizes. It should be noted that while 78% of the number of particles are less than 50 nm in this work and likely would show a spectrum of size dependent phase transitions based on #3 and #4, the volume of liquid metal in the system that these smaller particles make up is less than 15% only, which likely masks their behavior. Future studies could explore these smaller particles and the ability to further tune the phase behavior of the slurry. For smaller particles a greater deviation could be observed even beyond what is presented here, where the explanations #3 and #4 could lead to increased discrepancies and possibly more diverse phase formations from the effect of explanation #1s.

These PCM slurries demonstrate tunable and improved thermal behaviors. Phase change windows can be further adjusted by modifying the nanoparticle size distributions, composition changes and loading variations, as introduced here with various Ga/In ratios and loading amounts. The onset of melting and the associated latent heat can be adjusted to coincide with specific vulnerable temperature thresholds of sensitive high-power electronics. Materials such as these represent useful additives to traditional thermal fluids which increase the thermal conductivities up to nearly 50% with 10 vol.% nanoparticles and increase in thermal energy storage via reversible phase transformations. Future embodiments of such materials can be extended to encompass additional gallium-based alloys as well as other low melting alloys such

as Field's metal to further tune the working temperature range as well as potentially adding functionalities, including surface-bound reactive, magnetic, or electronically active species.

Experimental Section

Ga-In PCM Nanoslurry Production: Bulk Ga-In liquid metal of each composition was produced by mixing 99.999% gallium shot with 99.999% indium shot in 60 mL glass vials then heating to approximately 70℃ in a water bath. A 0.1 mL droplet of bulk liquid metal was then transferred to a standard 28 mm OD borosilicate glass scintillation vial filled with 15 mL of ethanol. Nanoparticles were produced via probe-tip ultrasonication at 30% amplitude (max power: 500 W) in a 10℃ (60℃ for 30-40 wt.% In) chilled water bath with the probe-tip breaching the ethanol surface by approximately 1 cm, as depicted by Figure 1A. From this mixture, a single droplet was then taken for particle size measurements and the remainder was transferred to a specified amount of Sigma-Aldrich supplied AR-200 silicone oil in a standard 28 mm OD borosilicate glass scintillation vial. The mixture was held under 25 mm-Hg of vacuum for 10-48 hours to selectively evaporate the ethanol, leaving behind the Ga-In PCM nanoslurry.

Particle Size Characterization: A droplet of the previously mentioned ethanol/nanoparticle mixture (before dispersion into AR-200) was diluted 100x with dichloromethane and then deposited on an ultrathin (3-4 nm) carbon film on 400-mesh copper grid purchased from Electron Microscopy Sciences (CF400-Cu-UL). Nanoparticle sizes and size distributions were measured by manually counting over 300 particles spread among several grid locations similar to the procedure of Yamaguchi et al.[29] A FEI Talos transmission electron microscope operating at 200 keV was used for particle sizing measurements.

Thermal Analysis: Differential scanning calorimetry (DSC) was utilized to locate phase transformations, latent heat of melting and fusion, and heat capacities. Thermal Analysis instruments (two model 2500s, two Q-100, one Q-1000) were used; the Q-100s were used exclusively with a liquid nitrogen cooling system to obtain temperatures below -90℃. DSC samples containing nanoparticles dispersed in heat transfer fluid (as opposed to solely nanoparticles) were compared to their respective thermal fluid reference or air reference in hermetically sealed aluminum pans. Bulk liquid metal measurements were measured using graphite pans with loose lids.

A HotDisk TPS 2500 system with a 2.5 mL Teflon fluid cavity and 3.189 mm diameter Hot Disk Kapton-coated sensor facilitated thermal conductivity measurements. Data for the Ga-In PCM nanoslurry was acquired using 40 s of the measurement time and 20 mW of heating power between 22℃ to 24℃. Measurement times were varied between 5 to 80 s and it was determined that 40 s was most appropriate due to the high viscosity of the sample (≥200 mPas). A set of eight measurements with thirty minutes of elapsed time in-between were acquired; error bars represent one standard deviation.

Rheological Analysis:

Parallel plate rheology was used to observe the rheological response and changes in viscosity of Ga-In PCM nanoslurries. A Thermal Instruments ARES-G2 was used with two 25 mm disposable steel plates with a plate gap from 0.5 mm to 0.65 mm. Shear rate was cycled three times between 0.1 Hz to 1000 Hz. Temperature was maintained at 25℃ via an integrated Peltier heating/cooling system.

Supporting Information

Supporting Information with more detailed particle sizing analysis, experimental procedures, and thermal analysis is available.

Acknowledgements

This work is supported in part by the US Air Force Office of Scientific Research under grant number FA9550-16-1-0087, titled Avian-Inspired Multifunctional Morphing Vehicles monitored by Dr. B. L. Lee. The authors would also like to thank Professor Melissa Grunlan and Ping Dong (TAMU Biomedical Engineering) for follow-up DSC tests.

References

[1] A. L. Moore and L. Shi, "Emerging challenges and materials for thermal management of electronics," *Mater. Today*, vol. 17, no. 4, pp. 163–174, 2014.

[2] M. Bahiraei and S. Heshmatian, "Electronics cooling with nanofluids: A critical review," *Energy Convers. Manag.*, vol. 172, pp. 438–456, Sep. 2018.

[3] B. Borgmeyer and H. B. Ma, "Experimental investigation of oscillating motions in a flat plate pulsating heat pipe," *J. Thermophys. Heat Transf.*, vol. 21, no. 2, pp. 405–409, 2007.

[4] S. K. Das, S. U. S. S. Choi, and H. E. Patel, "Heat transfer in nanofluids - A review," *Heat Transf. Eng.*, vol. 27, no. 10, pp. 3–19, 2006.

[5] V. Trisaksri and S. Wongwises, "Critical review of heat transfer characteristics of nanofluids," *Renew. Sustain. energy Rev.*, vol. 11, no. 3, pp. 512–523, 2007.

[6] S. Kakaç and A. Pramuanjaroenkij, "Review of convective heat transfer enhancement with nanofluids," *Int. J. Heat Mass Transf.*, vol. 52, no. 13–14, pp. 3187–3196, 2009.

[7] H. Inaba, "New challenge in advanced thermal energy transportation using functionally thermal fluids," *Int. J. Therm. Sci.*, vol. 39, no. 9–11, pp. 991–1003, Oct. 2000.

[8] Z. Chen and G. Fang, "Preparation and heat transfer characteristics of microencapsulated phase change material slurry: a review," *Renew. Sustain. Energy Rev.*, vol. 15, no. 9, pp. 4624–4632, 2011.

[9] M. Delgado, A. Lázaro, J. Mazo, and B. Zalba, "Review on phase change material emulsions and microencapsulated phase change material slurries: Materials, heat transfer studies and applications," *Renew. Sustain. Energy Rev.*, vol. 16, no. 1, pp. 253–273, 2012.

[10] Y. E. Milián, A. Gutiérrez, M. Grágeda, and S. Ushak, "A review on encapsulation techniques for inorganic phase change materials and the influence on their thermophysical properties," *Renew. Sustain. Energy Rev.*, vol. 73, pp. 983–999, Jun. 2017.

[11] A. Sharma, V. V. Tyagi, C. R. Chen, and D. Buddhi, "Review on thermal energy storage with phase change materials and applications," *Renew. Sustain. Energy Rev.*, vol. 13, no. 2, pp. 318–345, Feb. 2009.

[12] N. Xie, Z. Huang, Z. Luo, X. Gao, Y. Fang, and Z. Zhang, "Inorganic salt hydrate for thermal energy storage," *Appl. Sci.*, vol. 7, no. 12, 2017.

[13] C. R. Raj, S. Suresh, R. R. Bhavsar, V. Kumar Singh, and S. Reddy, "Effect of nano-gallium capsules on thermal energy storage characteristics of manganese organometallic SS-PCM," *Thermochim. Acta*, vol. 680, p. 178341, Oct. 2019.

[14] K. Kashiyama *et al.*, " Ga-Based Microencapsulated Phase Change Material for Low-Temperature Thermal Management Applications ," *Energy Storage*, no. February, pp. 1–8, 2020.

[15] T. Daeneke *et al.*, "Liquid metals: Fundamentals and applications in chemistry," *Chem. Soc. Rev.*, vol. 47, no. 11, pp. 4073–4111, 2018.

[16] C. J. Thrasher, Z. J. Farrell, N. J. Morris, C. L. Willey, and C. E. Tabor, "Mechanoresponsive Polymerized Liquid Metal Networks," *Adv. Mater.*, vol. 31, no. 40, pp. 1–8, 2019.

[17] B. J. Blaiszik, A. R. Jones, N. R. Sottos, and S. R. White, "Microencapsulation of gallium--indium (Ga--In) liquid metal for self-healing applications," *J. Microencapsul.*, vol. 31, no. 4, pp. 350–354, 2014.

[18] M. Wang, C. Trlica, M. R. Khan, M. D. Dickey, and J. J. Adams, "A reconfigurable liquid metal antenna driven by electrochemically controlled capillarity," *J. Appl. Phys.*, vol. 117, no. 19, 2015.

[19] S. Çlnar, I. D. Tevis, J. Chen, and M. Thuo, "Mechanical Fracturing of Core-Shell Undercooled Metal Particles for Heat-Free Soldering," *Sci. Rep.*, vol. 6, no. February, pp. 1–10, 2016.

[20] A. Martin *et al.*, "Heat-Free Fabrication of Metallic Interconnects for Flexible/Wearable Devices," *Adv. Funct. Mater.*, vol. 29, no. 40, pp. 1–9, 2019.

[21] A. Martin, C. Du, A. M. Pauls, T. Ward, and M. Thuo, "Polydispersity-Driven Printing of Conformal Solid Metal Traces on Non-Adhering Biological Surfaces," *Adv. Mater. Interfaces*, vol. 1, no. 1, pp. 1–7, 2020.

[22] M. D. Bartlett *et al.*, "High thermal conductivity in soft elastomers with elongated liquid metal inclusions," *Proc. Natl. Acad. Sci.*, vol. 114, no. 9, pp. 2143–2148, Feb. 2017.

[23] X. Huang, Z. Ren, and C. Majidi, "Soft Thermal Actuators with Embedded Liquid Metal Microdroplets for Improved Heat Management," *2020 3rd IEEE Int. Conf. Soft Robot. RoboSoft 2020*, pp. 367–372, 2020.

[24] D. Hartl, J. Mingear, B. Bielefeldt, J. Rohmer, J. Zamarripa, and A. Elwany, "Towards High-Frequency Shape Memory Alloy Actuators Incorporating Liquid Metal Energy Circuits," *Shape Mem. Superelasticity*, vol. 3, no. 4, pp. 457–466, 2017.

[25] Z. J. Farrell and C. Tabor, "Control of gallium oxide growth on liquid metal eutectic gallium/indium nanoparticles via thiolation," *Langmuir*, vol. 34, no. 1, pp. 234–240, 2017.

[26] T. R. Lear, S.-H. H. Hyun, J. W. Boley, E. L. White, D. H. Thompson, and R. K. Kramer, "Liquid metal particle popping: Macroscale to nanoscale," *Extrem. Mech. Lett.*, vol. 13, pp. 126–134, 2017.

[27] J. W. Boley, E. L. White, and R. K. Kramer, "Mechanically sintered gallium-indium nanoparticles," *Adv. Mater.*, vol. 27, no. 14, pp. 2355–2360, 2015.

[28] N. J. Morris, Z. J. Farrell, and C. E. Tabor, "Chemically modifying the mechanical properties of core-shell liquid metal nanoparticles," *Nanoscale*, vol. 11, no. 37, pp. 17308–17318, 2019.

[29] A. Yamaguchi, Y. Mashima, and T. Iyoda, "Reversible Size Control of Liquid-Metal Nanoparticles under Ultrasonication," *Angew. Chemie Int. Ed.*, vol. 54, no. 43, pp. 12809–12813, 2015.

[30] X. Meng Chen, G. Tao Fei, X. Feng Li, K. Zheng, and L. De Zhang, "Metastable phases in GalliumIndium eutectic alloy particles and their size dependence," *J. Phys. Chem. Solids*, vol. 71, no. 6, pp. 918–921, 2010.

[31] A. Martin, C. Du, B. Chang, and M. Thuo, "Complexity and Opportunities in Liquid Metal Surface Oxides," *Chem.*

Mater., 2020.
[32] T. Allen, *Particle size measurement*. Springer, 2013.
[33] J. C. Berg, *An introduction to interfaces & colloids: the bridge to nanoscience*. World Scientific, 2010.
[34] J. H. Gaddum, "Lognormal Distributions," *Nature*, no. 3964, pp. 463–466, 1945.
[35] H. A. Barnes, "Thixotropy—a review," *J. Nonnewton. Fluid Mech.*, vol. 70, no. 1–2, pp. 1–33, 1997.
[36] R. D. Heyding, W. Keeney, and S. L. Segel, "Metastable phases in gallium dispersions," *J. Phys. Chem. Solids*, vol. 34, no. 1, pp. 133–136, 1973.
[37] A. Defrain, "États métastables du gallium. Surfusion et polymorphisme," *J. Chim. Phys.*, vol. 74, pp. 851–862, May 1977.
[38] A. Di Cicco, "Phase Transitions in Confined Gallium Droplets," *Phys. Rev. Lett.*, 1998.
[39] A. Di Cicco, S. Fusari, and S. Stizza, "Phase transitions and undercooling in confined gallium," *Philos. Mag. B*, vol. 79, no. 11–12, pp. 2113–2120, 1999.
[40] H. He *et al.*, "Relation between size and phase structure of gallium: Differential scanning calorimeter experiments," *Phys. Rev. B*, vol. 72, no. 7, p. 73310, 2005.
[41] S.-Y. Tang *et al.*, "Phase Separation in Liquid Metal Nanoparticles," *Matter*, pp. 1–13, 2019.
[42] W. J. Boettinger, U. R. Kattner, K.-W. Moon, and J. H. Perepezko, "DTA and Heat-Flux DSC Measurements of Alloy Melting and Freezing," *Methods Phase Diagr. Determ.*, pp. 151–221, 2008.
[43] T. J. Anderson and I. Ansara, "The Ga-In (gallium-indium) system," *J. phase equilibria*, vol. 12, no. 1, pp. 64–72, 1991.
[44] S. Delcroix, A. Defrain, and I. Epelboin, "Sur les diagrammes d'alliages du gallium I ou II avec l'étain, le zinc ou l'indium," *J. Phys. le Radium*, vol. 24, no. 1, pp. 17–20, 1963.
[45] F. Calvo, "Thermodynamics of nanoalloys," *Phys. Chem. Chem. Phys.*, vol. 17, no. 42, pp. 27922–27939, 2015.
[46] G. B. Parravicini *et al.*, "Extreme undercooling (down to 90 K) of liquid metal nanoparticles," *Appl. Phys. Lett.*, vol. 89, no. 3, p. 33123, 2006.
[47] M. Yarema *et al.*, "Monodisperse colloidal gallium nanoparticles: synthesis, low temperature crystallization, surface plasmon resonance and Li-ion storage," *J. Am. Chem. Soc.*, vol. 136, no. 35, pp. 12422–12430, 2014.
[48] M. H. Malakooti *et al.*, "Liquid Metal Supercooling for Low-Temperature Thermoelectric Wearables," *Adv. Funct. Mater.*, vol. 29, no. 45, pp. 1–9, 2019.
[49] M. Losurdo, A. Suvorova, S. Rubanov, K. Hingerl, and A. S. Brown, "Thermally stable coexistence of liquid and solid phases in gallium nanoparticles," *Nat. Mater.*, vol. 15, no. 9, p. 995, 2016.
[50] W. D. Callister and D. G. Rethwisch, *Fundamentals of materials science and engineering*, 4th ed. John Wiley & Sons, Inc., 2012.
[51] K. K. Nanda, "Size-dependent melting of nanoparticles: Hundred years of thermodynamic model," *Pramana*, vol. 72, no. 4, pp. 617–628, 2009.
[52] K. K. Nanda, S. N. Sahu, and S. N. Behera, "Liquid-drop model for the size-dependent melting of low-dimensional systems," *Phys. Rev. A - At. Mol. Opt. Phys.*, vol. 66, no. 1, pp. 132081–132088, 2002.
[53] C. Q. Sun, Y. Wang, B. K. Tay, S. Li, H. Huang, and Y. B. Zhang, "Correlation between the melting point of a nanosolid and the cohesive energy of a surface atom," *J. Phys. Chem. B*, vol. 106, no. 41, pp. 10701–10705, 2002.
[54] J. Buongiorno *et al.*, "A benchmark study on the thermal conductivity of nanofluids," *J. Appl. Phys.*, vol. 106, no. 9, 2009.
[55] V. Y. Prokhorenko, V. V. Roshchupkin, M. A. Pokrasin, S. V. Prokhorenko, and V. V. Kotov, "Liquid gallium: potential uses as a heat-transfer agent," *High Temp.*, vol. 38, no. 6, pp. 954–968, 2000.